VII International Conference on Computational Methods for Coupled Problems in Science and Engineering
COUPLED PROBLEMS 2017
M. Papadrakakis, E. Oñate and B. Schrefler (Eds)

APPLICATION OF THE MODIFIED FINITE PARTICLE METHOD TO THE SIMULATION OF THE CORNEAL AIR PUFF TEST

ANDREA MONTANINO*, MAURIZIO ANGELILLO† AND ANNA PANDOLFI*

*Dipartimento di Ingegneria Civile ed Ambientale (DICA)
Politecnico di Milano
Piazza Leonardo da Vinci, 32, 20133 Milano, Italy
e-mail: {andrea.montanino, anna.pandolfi}@polimi.it

†Dipartimento di Ingegneria Civile (DiCiv)
Universitá degli Studi di Salerno,
Via Giovanni Paolo II, 84084 Fisciano (SA), Italy
e-mail: mangelillo@unisa.it

Key words: Meshless methods, air puff test, Fluid-Structure Interaction

Abstract. We present a numerical procedure for the simulation of the air puff test, a medical procedure used by ophtalmologists for the identification of the Intra Ocular Pressure, and potentially useful for the identification of material properties of the human cornea.

The problem involves the modeling of the cornea, that is a biological tissue, modelled as an hyperelastic material, and the aqueous humor, that is, the fluid filling the anterior chamber of the eye, that is treated as a Newtonian fluid, and modelled using a meshfree formulation, useful for the solution of a Fluid-Structure Interaction problem. Fluid and Structure are coupled using a Dirichlet-Neumann iterative approach, which permits the adoption of a partitioned coupling approach and explicit, fast solvers for the different subproblems.

1 Introduction

The identification of the in-vivo mechanical properties of the external part of the eye is a hot topic in the current literature, since the availability of a patient-specific model of the anterior chamber of eye will open new perspectives in improving the prevalence of positive outcomes of corneal refractive surgery.

In-vivo material properties must be determined necessarily by means of static or dynamic test performed on the external surface of the eye. The most promising tests are

based on the analysis of the dynamic deformation of the cornea induced by a localized time varying pressure. Advanced optical instruments, such as Ocular Response Analyzer (ORA; Reichert, Inc., Buffalo, NY) and Corvis ST (Oculus Optikgerate GmbH, Wetzlar, Germany), use a rapid single air jet which determines the cornea to snap from its original convex shape to a locally concave shape and back, passing through two configurations characterized by a localized flattened zone. The inward deflection is contrasted by the presence of filling fluids (aqueous humor). To provide a correct interpretation of the air puff test and, consequently, to measure from it significant mechanical parameters, it is necessary to develop a numerical model of the eye that accounts for several aspects, i. e.: (i) the exact geometry of the eye [1]; (ii) the use of reliable material models for the tissues [2, 3]; (iii) the fluid-structure interaction [4, 5]; (iv) the presence of surrounding tissues and of optical muscles at the limbus; (iv) the patient-specific fibril organization in the corneal tissue [6].

Recent works [7, 8] pointed out clearly that in order to capture the correct dynamics of the cornea, the air puff test model must include the interaction between the posterior filling fluids and the cornea. It follows that the characterization of the material parameters requires the use of identification algorithms based on advanced stress analysis procedures that can handle solid-fluid interactions.

The numerical approaches presented to date in the literature make use of advanced models of the human cornea, but in general the aqueous humor is not modelled, with some exceptions [9, 10]. A few attempts to account for the presence of the fluid include the use of spring-like elements [11] or added masses [7].

In this study, we aim at modelling explicitly the interaction between aqueous and cornea to elucidate the influence of the fluid on the development of dynamics of the the air puff test. In particular, here we use an analytical structural model (membrane like) for the cornea and a Modified Finite Particle Method (MFPM) [12, 13] for the fluid. We consider an axis symmetric two-dimensional problem, and adopt a simplified Fung's material for the solid. The dynamics of the anterior chamber of the eye undergoing an air puff test is modelled as a fluid-structure interaction (FSI) problem. The solution is based on a partitioned approach, which exploits the advantages of using a structural model for the solid and a meshless discretization for the fluid.

2 Problem formulation

The cornea is modelled as an isotropic hyperelastic membrane, loaded by the physiological pressure of the aqueous humor. We assume a simplified axis-symmetric geometry, where the anterior chamber is modelled as a spherical sector, confined between a deformable anterior membrane of radius R and a rigid posterior support of radius r. The membrane stands for the cornea, while the posterior surface accounts for the iris support backed by the lens. The simplification reduces the analysis of the fluid motion to a two-dimensional problem and the study of the membrane to an one-dimensional problem. The reference configuration of the fluid, under the physiological pressure, is visualized in

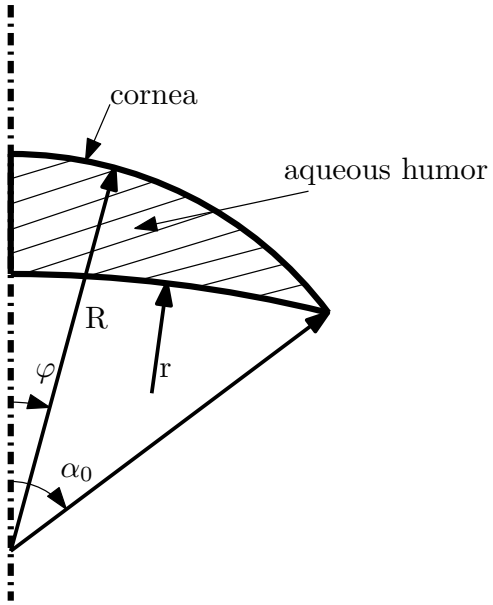

Figure 1: Reference geometry of the simplified model of the anterior chamber of the eye subject to the air puff test. The anterior surface is a deformable, circular membrane of radius R. The posterior surface is a rigid support of radius r.

Fig. 1.

2.1 Corneal membrane

The membrane representing the cornea is described as a circular arc of radius R, length $2\,R\alpha_0$, and thickness h, internally prestressed by the intraocular pressure (IOP) p_0, see Fig. 1. The effect of the air puff test is simulated with a space and time dependent air jet pressure p_a, acting from outside on the anterior surface of the cornea.

The membrane linear momentum balance equation reads

$$h\,\nabla\cdot\mathbf{P} + \mathbf{b}^0 = \rho_c\,h\,\ddot{\mathbf{u}}\,, \tag{1}$$

where ρ_c is the mass density of the cornea, $\mathbf{b}^0$ is the vector of external forces per unit area referred to the reference configuration, and $\mathbf{P}$ is the First Piola-Kirchhoff stress tensor, related to the membrane displacement through the hyperelelastic Fung's constitutive law. We assume that in any location of the cornea the external force is given by the algebraic sum of the fluid pressure p and of the time dependent air jet pressure $p_a = p_a(t)$.

The projection of Equation (1) on the tangential and radial directions gives

$$\frac{h}{R}\left(\frac{\cos\varphi}{\sin\varphi}(P_{11}-P_{22}) + P_{31} + P'_{11}\right) + b^0_1 - \rho_c h\ddot{u} = 0\,,$$
$$\frac{h}{R}\left(\frac{\cos\varphi}{\sin\varphi}P_{31} + P'_{31} - P_{11} - P_{22}\right) + b^0_3 - \rho_c h\ddot{w} = 0\,,$$

where b_1^0 and b_3^0 are the tangential and radial components of the external load, u and w are the membrane displacements along the tangential and radial directions.

2.2 Fluid aqueous humor

In order to facilitate the FSI coupling with the membrane, a Lagrangian approach is taken for the fluid. The aqueous humor is modelled as a Newtonian, weakly compressible fluid. In the present context, the weak compressibility assumption is justified by the possibility of using explicit time stepping algorithms for the integration of the fluid motion.

The governing equations for the fluid in a Lagrangian approach are

$$\rho_f \frac{d\,\mathbf{v}}{dt} = -\nabla p + \mu \nabla \mathbf{v}\,, \tag{2}$$

$$\frac{d\,\rho_f}{dt} = -\rho_f \nabla \cdot \mathbf{v}\,, \tag{3}$$

$$\frac{d\,\mathbf{x}}{dt} = \mathbf{v}\,, \tag{4}$$

where μ is the fluid viscosity, ρ_f the current fluid density, p the current fluid pressure, and $\mathbf{x}$ the fluid particle position. Eq. (2) is the linear momentum balance, Eq. (3) is the mass balance or continuity equation, and Eq. (4) is the definition of the fluid velocity.

Within a Lagrangian meshfree formalism and when explicit time stepping algorithms are adopted, a convenient way to approximate incompressibility is to introduce an equation of state that relates the fluid pressure to the speed of sound c. The set of equations is completed thus with the equation

$$p = p_0 + \frac{\rho_0\, c^2}{\gamma}\left[\left(\frac{\rho}{\rho_0}\right)^{\gamma} - 1\right]\,. \tag{5}$$

where ρ_0 is the reference fluid density and p_0 are the reference fluid pressure. The speed c has to be seen as a numerical parameter rather than a physical parameter, and the chosen value should not be too large, to avoid exceedingly small time steps. For example, in the smoothed particle hydrodynamics (SPH) literature, a fictitious value of $c = 50$ m/s (in contrast to the physical value $c = 340$ m/s) is usually considered adequate for water [14].

3 Solution algorithm

The FSI problem is solved using a partitioned approach, which allows the use of suitable solvers both for the solid subproblem and the fluid subproblem.

The membrane problem is solved using a Finite Difference approximation; in the axis-symmetric approximation, the problem becomes one-dimensional. The circular arc domain $\varphi \in [0, \alpha_0]$ is discretized in N equi-spaced nodes. The spatial partial derivatives are discretized with standard central differences, while the time stepping algorithm is the explicit Verlet's method, belonging to the family of Newmark's methods.

The fluid domain is approximated using the Modified Finite Particle Method (MFPM), a meshless approach particularly suitable for the description of moving boundaries and FSI problems. The method consists in discretizing the differential operators at a discrete number of points of the domain (nodes). The aproximation technique for spatial differential operators of a funtion $f(\mathbf{x})$ at a generic point $\mathbf{x}_i$ is obtained through the projection of the Taylor series expansion of $f(\mathbf{x})$ (centered on $\mathbf{x}_i$ and evaluated at a certain number of neighboor nodes $\mathbf{x}_j$) on some "projection funtions" $W_\alpha(\mathbf{x}-\mathbf{x}_i)$. Further details of the algorithm can be found in the original papers [12, 13].

Time integration is achieved through the following algorithm. Let $\mathbf{x}^n$, $\mathbf{v}^n$, and ρ^n be the arrays containing position, velocity, and density of the nodes at the time step t_n. The algorithm begins by computing the quantities at mid-time step. The node position and density are computed through explicit forward Euler schemes as

$$\mathbf{x}^{n+1/2} = \mathbf{x}^n + \frac{\Delta t}{2}\mathbf{v}^n\,,$$

$$\rho^{n+1/2} = \rho^n - \frac{\Delta t}{2}\rho^n\,\nabla^n\cdot\mathbf{v}^n\,,$$

where $\nabla^n\cdot$ denotes the discrete divergence at t^n, and the mid-time step fluid pressure $p^{n+1/2}$ is evaluated through eq. (5). The velocity at the time t_{n+1} is computed by using the half-step discrete differential operator $\nabla^{n+1/2}$ as

$$\mathbf{v}^{n+1} = \mathbf{v}^n - \frac{\Delta t}{\rho^{n+1/2}}\nabla^{n+1/2}p^{n+1/2} + \mu\,\frac{\Delta t}{\rho^n}\,\nabla^{n2}\mathbf{v}^n\,.$$

The node position and the density are then updated as

$$\mathbf{x}^{n+1} = \mathbf{x}^{n+1/2} + \frac{\Delta t}{2}\mathbf{v}^{n+1}\,,$$

$$\rho^{n+1} = \rho^{n+1/2} - \frac{\Delta t}{2}\rho^{n+1/2}\,\nabla^{n+1}\cdot\mathbf{v}^{n+1}\,,$$

using an explicit advance in time for density using the velocity at the final time step $n+1$. The pressure p^{n+1} is then computed through eq. (5). The algorithm is second-order accurate in the pressures, and first order accurate in the velocities.

The coupling algorithm consists in solving first the solid problem, by imposing, as external loads for the membrane, both the external and the fluid pressure. The membrane velocity is then passed to the fluid solver and imposed as boundary condition for the fluid domain. The fluid pressure at the membrane is then computed, and the procedure is completed if the following condition is respected

$$\frac{\|\mathbf{p}_i^k - \mathbf{p}_i^{k-1}\|}{\|\mathbf{p}_i^{k-1}\|} < \varepsilon \tag{6}$$

where $\mathbf{p}_i^k$ and $\mathbf{p}_i^{k+1}$ are the fluid pressure values at the fluid-solid interface points at time t_i and at two subsequent iterations k and $k+1$, and ε is the desired tolerance. In the present calculations ε is set 10^{-4}.

If Equation (6) is not respected, the new fluid pressure is imposed as external load for the membrane, and the pricedure is repeated untill convergence.

4 Application: the air puff test

The air puff test is a clinical procedure used by ophthalmologists to measure the Intra-Ocular Pressure (IOP). It consists in a rapid air jet pulse that hits the external surface of the cornea, determining the snap of the cornea from its original, convex shape to a temporary, local concave configuration.

The interpretation of the test is made through two instruments: Corvis ST and the Ocular Response Analyzer (ORA) [15]. In particular, Corvis ST, besides the value of IOP, provides kinematic data, such as the displacement u of the apical point of the cornea versus time t. The results are shown in Figure 2(a)

The Ocular Response Analyzer (ORA), instead, returns a number of pressure parameters recorded during the test:

1. P1 and P2 (expressed in mmHg), i.e., the instrument pressures registered at the two times corresponding to the applanation state of the cornea (the first, when the cornea is moving inward switching from convex to concave configuration, and the second, when the cornea is moving outward switching from concave to convex configuration);

2. the Corneal Hysteresis, measured as CH = P1 − P2;

3. the Goldmann equivalent IOP, measured as IOPg = 0.5 (P1 + P2);

4. the Corneal Compensated IOP, measured as IOPcc = P1 − 0.43 P2.

The results of ORA are usually shown in graphs similar to that reported in Figure 2(b), in which the two instant of local applanation are evident.

Though Corvis ST does not provide a pressure profile, the results given by Corvis ST can be reprocessed by using an artificial pressure history of the type

$$p(t) = p_{\max} \exp\left[-b\,(t - t_0)^2/T^2\right]; \tag{7}$$

where $T = 30$ ms is the total duration of the impulse (known), which reaches the peak value $p_{\max}$ at time $t_0 = 15$ ms. For the parameters, we use $b = 25$ [7, 8] and $p_{max} = 10$ kPa. In Figures 3 the pressure profile p is reported together with the apical displacement u versus time t. In Figure 4 the p-u relation is reconstructed. The hysteresis loop that can be seen in Figure 4 is essentially produced by inertial effects [7] and by the fluid viscosity.

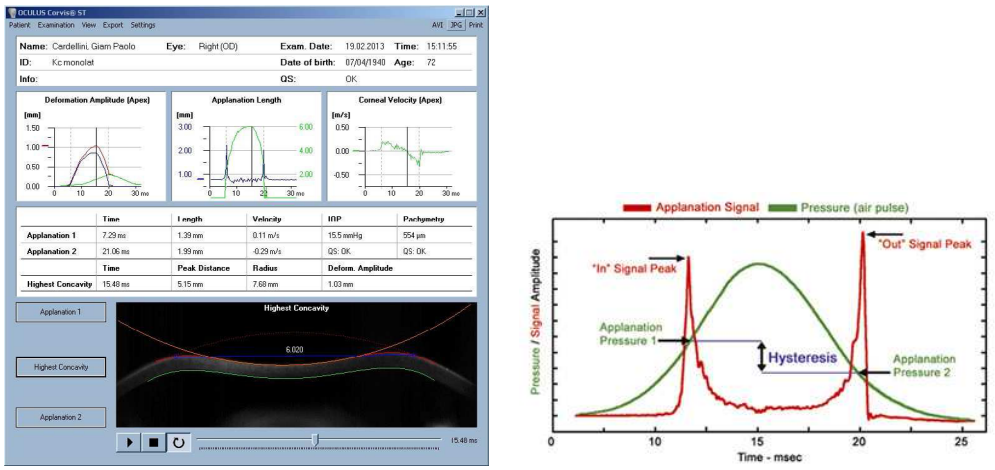

(a) (b)

Figure 2: (a) Example of sheet provided by the Corvis ST. (b) Example of sheet provided by the ORA

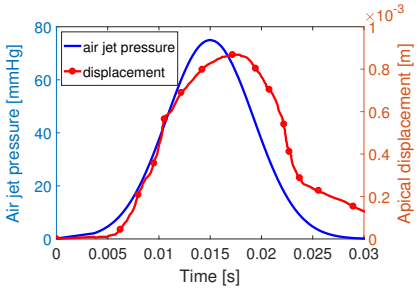

Figure 3: Experimental curves for the apical displacement and external air jet pressure versus time

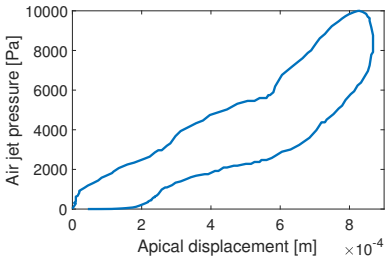

Figure 4: Experimental curve of the air jet pressure versus the apical displacement.

5 Numerical simulations

The model of the cornea is used to simulate the ORA test, using reference parameters. The density of the cornea is similar to the one of the water, $\rho = 1$ kg/m^3. An estimate of the elastic modulus $E_0 = 0.5$ MPa is obtained by fitting with the present material model the numerical results documented in [7], where a sophisticated material model of the cornea has been used to simulate the air puff test. The reference density ρ_0 and pressure p_0 (IOP) of the fluid are assumed to be $\rho_0 = 1$ kg/m^3 and $p_0 = 16$ mmHg (2.14 kPa), a value in the range 12-21 mmHg of the physiological IOP.

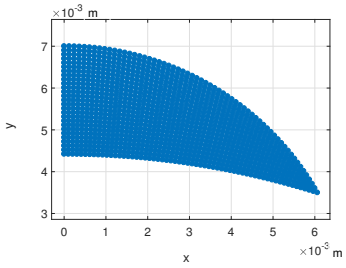

Figure 5: Reference node distribution for the fluid domain

In numerical simulations we consider an ideal geometry of the anterior chamber, characterized by the parameters $R = 7$ mm, $r = 2.04$ mm, $h = 0.5$ mm, and $\alpha_0 = \pi/3$. The posterior surface of the anterior chamber (i.e., the iris) containing the fluid is assumed to be rigid. The fluid is discretized in 1134 nodes, see Fig. 5.

We assume axis-symmetry boundary conditions for both fluid and membrane, by setting on the symmetry axis

$$u = 0\,, \qquad w' = 0 \quad \text{at} \quad x = 0\,, \tag{8}$$

and

$$v_x = 0\,, \qquad \frac{\partial v_y}{\partial x} = 0 \quad \text{at} \quad x = 0\,, \tag{9}$$

being the v_x and v_y the fluid velocity components along the x and y axes.

The point representing the limbus (intersection between anterior and posterior surface) is fixed:

$$u = 0\,, \qquad w = 0 \quad \text{at} \quad \varphi = \frac{\pi}{3}\,. \tag{10}$$

The anterior surface of the cornea is loaded quickly with an impulsive air-jet with pressure history

$$p(t) = p_{\max} \exp\left[-a \, \sin^2 \varphi\right] \exp\left[-b\,(t - t_0)^2/T^2\right]; \tag{11}$$

where $T = 30$ ms is the total duration of the impulse, which reaches the peak value $p_{\max}$ at time $t_0 = 15$ ms. We assume $a = 21.5$, $b = 25$ [7, 8]

The sound speed c appearing in eq. (5) is chosen to enforce the quasi-incompressibility of the fluid and thus it varies with the time step, according to the expression $c = 10 + 20v_{max}$ m/s, where v_{max} is the maximum norm of the value of the fluid velocity magnitude at the previous time step.

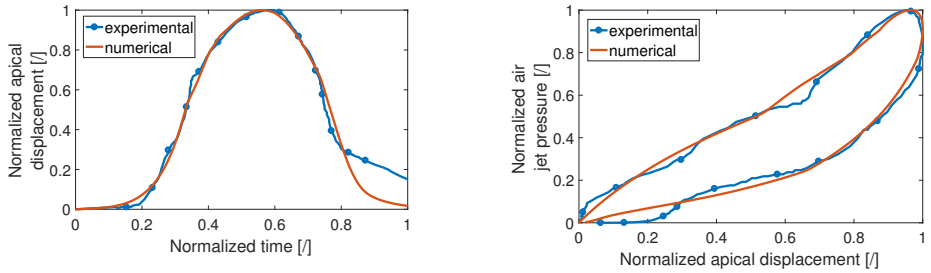

(a) (b)

Figure 6: Comparison with experimental data: (a) Apex displacement versus time. (b) Apex displacement versus air jet pressure.

The output of the analysis are rendered through Figures 6(a) (in terms of normalized displacement and normalized time) and Figures 6(b) (in terms of normalized displacement and normalized pressure), in which also is shown the comparison between the experimental data introduced in Section 4 and the numerical simulation.

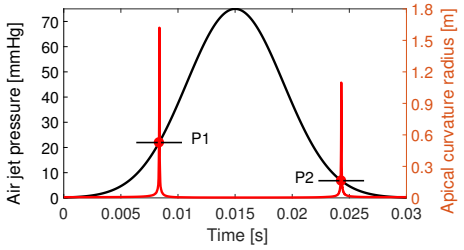

Figure 7: Baseline analysis: corneal applanated states

Fig. 7 visualizes the time history of the air jet pressure and of the corneal curvature at the apex. For the baseline analysis we obtain the following values P1=21.96 mmHg, P2=6.82 mmHg, CH=15.14 mmHg, IOPg=14.39 mmHg, and IOPcc=19.03 mmHg.

The effects of the dynamics of the fluid can be clearly seen in Figure 8, in which we plot the apical displacement and the external air jet pressure versus time. We notice that the maximum apical displacement occurs with some delay with respect to the maximum of the air jet pressure.

We also show, for qualitative comparison, some images taken from the Corvis instrument during an air puff test (Figure 9) with the results of our simulation for the baseline analysis (Figure 10).

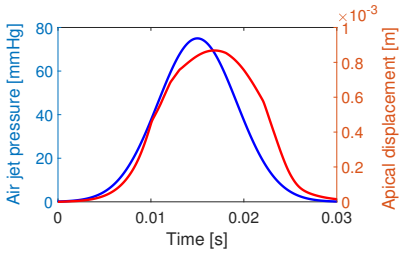

Figure 8: Baseline analysis: external air jet pressure and apical displacement versus time

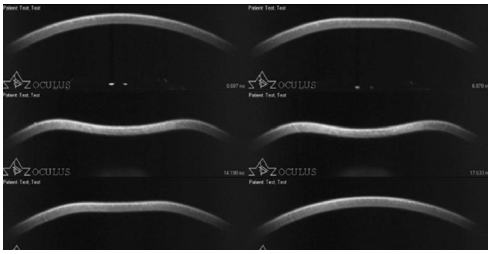

Figure 9: Images recorded by the instrument Corvis ST during an air puff test (from the web)

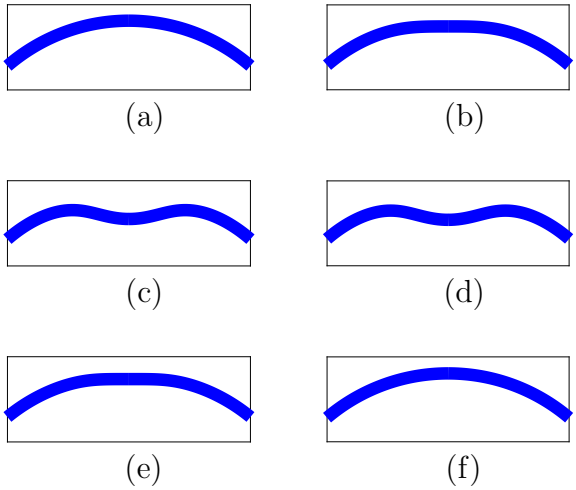

Figure 10: Deformed configurations of the cornea obtained with the baseline analysis: (a) undeformed, physiological configuration; (b) first applanation; (c) deformed configuration during the maximum air jet pressure; (d) deformed configuration at the maximum apical displacement; (e) second applanation; (f) new physiological configuration after the test

6 Conclusion

In the present work we present the simulation of the air puff test using a Fluid Structure Interaction approach. The problem is approached with a partitioned strategy, preserving the efficiency of the different solvers for the solid and fluid part.

The problem is formulated exploiting axial-symmetry: thus, the solid problem becomes one dimensional, and is solved with Finite Differences, and using an explicit Verlet algorithm for the time advance. The fluid problem is solved using a meshfree Modified Finite Particle Method, particularly suitable for the solution of problems with moving boundaries and Fluid Structure Interaction. The coupling algorithm is an iterative Dirichlet-Neumann procedure, which allows the use of suitable solver preserving a strong coupling between the two problems.

W finally observe the evaluability of our numerical simulations, in terms of adherence between the experimental and numerical results, and in terms of efficiency of the numerical approach, thanks to the wide use of explicit algorithms.

References

[1] I. Simonini and A. Pandolfi. Customized finite element modelling of the human cornea. *PLoS ONE*, 10(6):e0130426, 2015. doi: 10.1371/journal.pone.0130426.

[2] A. Pandolfi and F. Manganiello. A material model for the human cornea. *Biomechanics and Modelling in Mechanobiology*, 5:237–246, 2006.

[3] P. Sánchez, K. Moutsouris, and A. Pandolfi. Biomechanical and optical behavior of human corneas before and after photorefractive keratectomy. *Journal of Cataract & Refractive Surgery*, 40(6):905–917, 2014.

[4] M. A. Ariza-Gracia, J. F. Zurita, J. F. Piñero, D. P. ad Rodriguez-Matas, and B. Calvo. Coupled biomechanical response of the cornea assessed by non-contact tonometry. A simulation study. *PLoS ONE*, 10(3):e0121486, 2015.

[5] A. Sinha Roy, M. Kurian, H. Matalia, and R. Shetty. Air-puff associated quantification of non-linear biomechanical properties of the human cornea in vivo. *Journal of the Mechanical Behavior of Medical Biomaterials*, 48(1):173–182, 2015.

[6] A. Pandolfi and M. Vasta. Fiber distributed hyperelastic modeling of biological tissues. *Mechanics of Materials*, 44:151–162, 2012.

[7] Irene Simonini, Maurizio Angelillo, and Anna Pandolfi. Theoretical and numerical analysis of the corneal air puff test. *Journal of the Mechanics and Physics of Solids*, 93:118–134, 2016.

[8] I. Simonini and A. Pandolfi. The influence of intraocular pressure and air jet pressure on corneal contactless tonometry tests. *Journal of the Mechanical Behavior of Medical Biomaterials*, Online First(July):1–15, 2015. doi: http://dx.doi.org/10.1016/j.jmbbm.2015.07.030.

[9] L. Coquart, C. Depeursinge, A. Curnier, and R. Ohayon. A fluid-structure interaction problem in biomechanics: Prestressed vibrations of the eye by the finite element method. *Journal of Biomechanics*, 25(10):1105–1118, 1992. doi: 10.1016/0021-9290(92)90067-B. cited By 26.

[10] S. Salimi, S. Simon Park, and T. Freiheit. Dynamic response of intraocular pressure and biomechanical effects of the eye considering fluid-structure interaction. *Journal of Biomechanical Engineering*, 133(9), 2011. doi: 10.1115/1.4005166. cited By 6.

[11] S. Kling, N. Bekesi, C. Dorronsoro, D. Pascual, and S. Marcos. Corneal viscoelastic properties from finite-element analysis of in vivo air-puff deformation. *PLoS ONE*, 9 (8):e104904, 2014. doi: 10.1371/journal.pone.0104904.

[12] D Asprone, F Auricchio, A Montanino, and A Reali. A modified finite particle method: Multi-dimensional elasto-statics and dynamics. *International Journal for Numerical Methods in Engineering*, 99(1):1–25, 2014.

[13] D Asprone, F Auricchio, A Montanino, and A Reali. Review of the modified finite particle method and application to incompressible solids. *International Journal of Multiphysics*, 9(3), 2015.

[14] Joe J Monaghan. Simulating free surface flows with sph. *Journal of computational physics*, 110(2):399–406, 1994.

[15] D. A. Luce. Tonometer calibration tool, 01 2004. URL `http://www.google.com/patents/US6679842`.